RMetS

Royal Meteorological Society

An improvement in clear-air turbulence forecasting based on spontaneous imbalance theory: the ULTURB algorithm

Donald W. McCann,[a]* John A. Knox[b] and Paul D. Williams[c]

[a] *McCann Aviation Weather Research, Inc., Overland Park, KS, USA*
[b] *Department of Geography, University of Georgia, Athens, GA, USA*
[c] *Department of Meteorology, University of Reading, Reading, UK*

ABSTRACT: Recent research has shown that Lighthill–Ford spontaneous gravity wave generation theory, when applied to numerical model data, can help predict areas of clear-air turbulence. It is hypothesized that this is the case because spontaneously generated atmospheric gravity waves may initiate turbulence by locally modifying the stability and wind shear. As an improvement on the original research, this paper describes the creation of an 'operational' algorithm (ULTURB) with three modifications to the original method: (1) extending the altitude range for which the method is effective downward to the top of the boundary layer, (2) adding turbulent kinetic energy production from the environment to the locally produced turbulent kinetic energy production, and, (3) transforming turbulent kinetic energy dissipation to eddy dissipation rate, the turbulence metric becoming the worldwide 'standard'. In a comparison of ULTURB with the original method and with the Graphical Turbulence Guidance second version (GTG2) automated procedure for forecasting mid- and upper-level aircraft turbulence ULTURB performed better for all turbulence intensities. Since ULTURB, unlike GTG2, is founded on a self-consistent dynamical theory, it may offer forecasters better insight into the causes of the clear-air turbulence and may ultimately enhance its predictability. Copyright © 2011 Royal Meteorological Society

KEY WORDS   aviation weather; gravity waves; Lighthill–Ford

Received 27 April 2010; Revised 21 October 2010; Accepted 24 February 2011

1. Introduction

Ever since World War II, when aircraft began flying at higher altitudes and encountering turbulence in clear air, meteorologists have been trying to understand and forecast this phenomenon. Even though early research connected the cause of clear-air turbulence (CAT) with theories of atmospheric instability (Dutton and Panofsky, 1970), forecasters found it difficult to implement any technique resting on theoretical foundations. Instead, forecasters developed empirical rules and diagnostics based on their observations of atmospheric patterns when pilots reported turbulence, e.g. Dutton (1980) and Ellrod and Knapp (1992). Over several decades the forecast skill improvements were marginal (Sharman *et al.*, 2006).

Recognizing that no one technique has sufficient skill in the many weather patterns known to produce CAT, Sharman *et al.* (2006) developed the Graphical Turbulence Guidance (GTG) method. GTG is a statistical forecast based on a weighting of a set of previously used diagnostics determined to have some skill in CAT forecasting. The GTG finds the best weighting of the diagnostics associated with the observations, pilot reports (PIREPs), and uses that weighting in a forecast model.

Although the GTG verifies better than any of its input CAT diagnostics, as a combination of many diagnostics, it fails to give much physical insight into the causes of the turbulence.

Knox *et al.* (2008, hereafter KMW) introduced a new clear-air turbulence forecast method based on McCann's (2001) theoretical ingredients-based forecast technique. The technique is founded on the idea that gravity waves may initiate turbulence. McCann's technique combines two ingredients, (1) the environmental Richardson number and its components, vertical temperature stability and vertical wind shear, and, (2) the non-dimensionalized amplitude of a gravity wave. Normally, above the boundary layer the environmental stability and wind shear are insufficient for turbulence to form, but gravity waves locally modify the stability and wind shear. These modified values may be sufficient for turbulence to develop.

The environmental Richardson number can be easily computed with observational or numerical model data, but the gravity wave non-dimensional amplitude is more problematic. Williams *et al.* (2005, 2008) associated Lighthill–Ford radiation (Lighthill, 1952; Ford, 1994) with spontaneous gravity wave production in their rotating annulus laboratory experiments. Motivated by Williams *et al.*'s results, KMW estimated gravity wave non-dimensional amplitudes from a numerical forecast model diagnostic of the Lighthill–Ford radiation. These were inserted into the McCann formulae and resulted in

* Correspondence to: D. W. McCann, McCann Aviation Weather Research, Inc., 7306 157th Terrace, Overland Park, KS 66223, USA. E-mail: don@mccannawr.com

successful CAT forecasts at flight levels (FL) at or above 20 000 ft (FL200).

It is noted in passing that Plougonven *et al.* (2009) have questioned KMW's use of Lighthill–Ford radiation as an indicator of gravity waves. In reply Knox *et al.* (2009) acknowledge that there are no direct observations linking Lighthill–Ford radiation and gravity wave generation other than those in Williams *et al.*'s experiments previously cited. However, the alternative explanation for its success suggested by Plougonven *et al.* (2009), frontogenesis, is insufficient and problematic. Frontogenesis is already incorporated, directly or indirectly, into many forecast methods, including GTG2 (Sharman *et al.*, 2006), that do not do as well as the KMW method because these deformation-based diagnostics frequently overforecast CAT and also miss CAT events caused by other forcing mechanisms (Knox, 1997). Moreover, Knox *et al.* (2009) show a major CAT outbreak case with diagnosed frontolysis. In short, to date there is no better account for the success of the KMW method than spontaneous generation of gravity waves. It is also noted that Plougonven *et al.* did not challenge the capability of the method and felt that it 'may well be very efficient and relevant'.

First, KMW's study is reviewed, and the method for computing turbulent kinetic energy (TKE) production/dissipation. After developing the method, it was tested, culminating in an improved algorithm, ULTURB (Upper Level TURBulence, i.e. any level above the boundary layer). Validation results show the ULTURB modifications to the KMW method yielded better forecasts. Additionally, comparisons of ULTURB forecasts with the second version of GTG (GTG2) reveal that ULTURB also outperforms GTG2 at all turbulence intensities, especially severe.

2. Review of the KMW method

TKE budget equations describe how turbulence is produced, transformed and dissipated. It was assumed that the TKE produced is eventually dissipated, a good assumption over a characteristic time and space much greater than the life and size of individual eddies, i.e. hours and tens of kilometres or the time and volume of typical aviation forecasts. Therefore, a simple, steady-state first-order closure TKE equation, found in many references on turbulence (e.g. Garratt, 1992), was used:

$$\varepsilon = K_m \left(\frac{\partial \mathbf{V}}{\partial z}\right)^2 - K_h \frac{g}{\Theta_v} \frac{\partial \Theta_v}{\partial z} \qquad (1)$$

where ε is TKE dissipation, K_m and K_h are eddy viscosity and eddy thermal diffusivity, respectively, $\mathbf{V}$ is the vector wind, g is the acceleration of gravity, and Θ_v is the virtual potential temperature. It was also assumed that the initially-produced turbulent eddies are at least as large as the approximately 10–1000 m inertial sub-range felt by aircraft, and that the TKE cascades through this range on the way to molecular dissipation.

Using the dispersion relationship for the vertically propagating gravity wave component (Dunkerton, 1997), the wave modifies the environmental wind shear to:

$$\left(\frac{\partial \mathbf{V}}{\partial z}\right)_{\mathrm{L}} = \left(\frac{\partial \mathbf{V}}{\partial z}\right)_{\mathrm{E}} \left(1 + Ri_{\mathrm{E}}^{1/2} \hat{a} \sin \varphi\right) \qquad (2)$$

and the wave modifies the environmental stability to:

$$N_{\mathrm{L}}^2 = N_{\mathrm{E}}^2 (1 + \hat{a} \cos \varphi) \qquad (3)$$

where the subscripts L and E indicate the local (modified) and environmental conditions, respectively, Ri is the Richardson number defined as the ratio of the stability, $N^2 = g \partial \Theta_v / \Theta_v \partial z$ to the wind shear squared, $\hat{a}$ is the wave's non-dimensional amplitude, $a N_{\mathrm{E}} / |\mathbf{V} - \mathbf{c}|$ (where a is the actual wave amplitude and the denominator is the wind velocity, Doppler adjusted for the wave phase velocity $\mathbf{c}$), and φ is the gravity wave phase angle.

McCann (2001) combined Equations (2) and (3) into a locally-modified Richardson number under the influence of the gravity wave:

$$Ri_{\mathrm{L}} = Ri_{\mathrm{E}} \frac{(1 + \hat{a} \cos \varphi)}{(1 + Ri_{\mathrm{E}}^{1/2} \hat{a} \sin \varphi)^2} \qquad (4)$$

The local Richardson number fluctuates within a gravity wave. Therefore, only portions of the wave are turbulent if Ri_{L} is low enough.

A necessary condition for turbulence to form is when $Ri < 0.25$ (Miles and Howard, 1964). So when $\varphi = \pi$ and $\hat{a} > 1$, we obtain $Ri_{\mathrm{L}} < 0.0$ and turbulence occurs. Similarly, when $\varphi = \pi/2$ and $\hat{a} > (2 - Ri_{\mathrm{E}}^{-1/2})$, we obtain $Ri_{\mathrm{L}} < 0.25$. Therefore, no matter how high the environmental Richardson number is, a gravity wave of sufficient amplitude may initiate turbulence. Also, the lower Ri_{E}, the weaker the gravity wave needs to be to initiate turbulence.

Inserting the gravity wave-modified wind shear and stability from Equations (2) and (3) each into Equation (1) and finding the maxima of each gives two estimates of local TKE dissipation:

$$\varepsilon_{\mathrm{wshr}} = K_m \left(\frac{\partial V}{\partial z}\right)_{\mathrm{L}}^2 \left(1 + \hat{a} \sqrt{Ri_{\mathrm{L}}}\right)^2 \qquad (5)$$

and

$$\varepsilon_{\mathrm{buoy}} = K_h (\hat{a} - 1) N_{\mathrm{L}}^2 \qquad (6)$$

due to wind shear and buoyancy, respectively. The eddy viscosity is empirically determined so that the resulting TKE dissipation estimates the turbulence intensity of actual aircraft (McCann, 1999; Pettegrew *et al.*, 2010). From Ri being less than 0.25 implying turbulence, $K_h = 4 K_m$. KMW used the maximum of $\varepsilon_{\mathrm{buoy}}$ and $\varepsilon_{\mathrm{wshr}}$ in their analyses, but the next section shows better results with a slight reinterpretation of the TKE equation.

Any type of gravity wave may force turbulence, but there is little, if any, knowledge of locations, wave amplitudes and wave phase velocities. Due to

the lack of consensus about inertia-gravity waves in theories and atmospheric observations, KMW sought guidance from laboratory rotating annulus experiments (Williams *et al.*, 2005, 2008). Observed gravity waves in the Williams *et al.* experiments best fit their calculations of Lighthill–Ford radiation. KMW expressed the Lighthill–Ford radiation equation in terms that could be computed on gridded atmospheric data, such as numerical forecast models:

$$R = f\mathbf{V} \cdot \nabla \zeta + 2Df\zeta - f\mathbf{k} \cdot \mathbf{V} \times \nabla D - 2\frac{\partial}{\partial t}J(u, v) \quad (7)$$

where R is the Lighthill–Ford radiation source term, f is the Coriolis parameter, D is the divergence, ζ is the vorticity, and u and v are components of the wind $\mathbf{V}$. The final term on the right hand side is the time derivative of the Jacobian of these components.

In small Rossby number ($Ro \ll 1$) environments typical of synoptic-scale flows, gravity wave amplitudes are proportional to the square root of R (KMW). Thus, by calculating R in Equation (7) from gridded data, â may be determined using proportionality constants, leading to calculation of TKE dissipation in Equations (5) and (6).

3. Modifications to KMW leading to ULTURB

3.1. CAT below FL200

Forecasting turbulence below FL200 is perceived to pose special problems. While the physical causes of turbulence are the same throughout the atmosphere, conditions for turbulence where aircraft fly vary greatly. Near the Earth's surface vertical temperature stability is often low so even with modest wind shears the boundary layer is often turbulent. Near jet streams, vertical wind shears can be large and, since wind speeds aloft typically increase with height to the tropopause, Lighthill–Ford radiation (Equation (7)) is often large in the stronger flow above FL200. Between the top of the boundary layer and FL200 or the low and mid level altitudes, these circumstances occur less often and probably in different scenarios. Sharman *et al.* (2006) found it necessary to create a different set of GTG diagnostics for FL100-FL200, and GTG does not forecast turbulence below FL100.

Returning to the PIREP database used in KMW and using the same rules, 3996 turbulence pilot reports below FL200 each day at 1500 UTC plus or minus 1 h between 3 November 2005 and 26 March 2006 were gathered. These were compared with TKE dissipation computed on the 1 h forecasts of the operational 20 km RUC2 numerical forecast model. Figure 1 shows Heidke Skill Scores (Doswell *et al.*, 1990) for light or greater and for moderate or greater turbulence PIREPs below FL200. The skill scores below FL200 are actually greater than those FL200 and above (results for PIREPs FL200 and above were computed from the KMW PIREP database). There were not enough severe PIREPs to stratify by altitude.

It is noted that the KMW method actually has greater skill at what is thought to be altitudes more difficult to forecast CAT. It is known that vertical wind shear is usually high in the vicinity of fronts aloft, but because positive vorticity and convergence are frequently observed near fronts, it is possible that Lighthill–Ford radiation is also high near many fronts.

3.2. A full accounting of the gravity wave-modified TKE equation

Subsequent to KMW, analyses of some cases of high TKE dissipation above FL400 suggested that values were too high. Since there were few clear-air turbulence PIREPs above FL400, complete analyses of these cases was not possible. However, a reasonable inference was that the very stable vertical temperature structure above the tropopause should be suppressing these high values. While looking for a probable cause, it was noticed that a solution might be found in the TKE equation itself.

The TKE dissipation in the KMW method is the greater of $\varepsilon_{\text{buoy}}$ and $\varepsilon_{\text{wshr}}$. However, at the gravity wave phase angle $\varphi = \pi$, when local buoyancy TKE dissipation is largest, from Equation (2) the environmental wind shear production is still positive, since $\sin \varphi = 0$. Likewise, when $\varphi = \pi/2$, when local wind shear production is largest, environmental buoyancy production must be accounted for. Since environmental buoyancy production is almost always negative, accounting for this suppresses the local wind shear production.

Thus, the net effect of a full accounting of the gravity wave-modified TKE equation is to increase TKE production/dissipation when the local buoyancy modification is greatest and to reduce TKE production/dissipation when the local wind shear production is greatest. This successfully reduced the apparent high bias in TKE dissipation forecasts above the tropopause. The local buoyancy modification only takes effect in situations with small vertical wind shear: otherwise, the local wind shear production would predominate. Therefore, adding the environmental wind shear production makes only small increases in $\varepsilon_{\text{buoy}}$. In the next section these results are validated.

3.3. TKE dissipation and eddy dissipation rate

In KMW turbulence intensity is expressed as turbulent kinetic energy dissipation *per* unit mass (Joules *per* second or $\text{m}^2 \text{ s}^{-3}$). However, the cube root of TKE dissipation, called eddy dissipation rate (EDR), has become the International Civil Aviation Organization's standard reporting metric (Cornman *et al.*, 2008). While it is easy to transform TKE dissipation into EDR, when KMW was written there was no standard mapping of EDR into subjective turbulence intensity (KMW showed TKE dissipation thresholds that maximized forecast skill which could be mapped into intensity). Since then, there have been enough EDR data to create a standard mapping (Pettegrew *et al.*, 2010, Table I), and so the KMW TKE dissipation has been transformed into EDR for ULTURB.
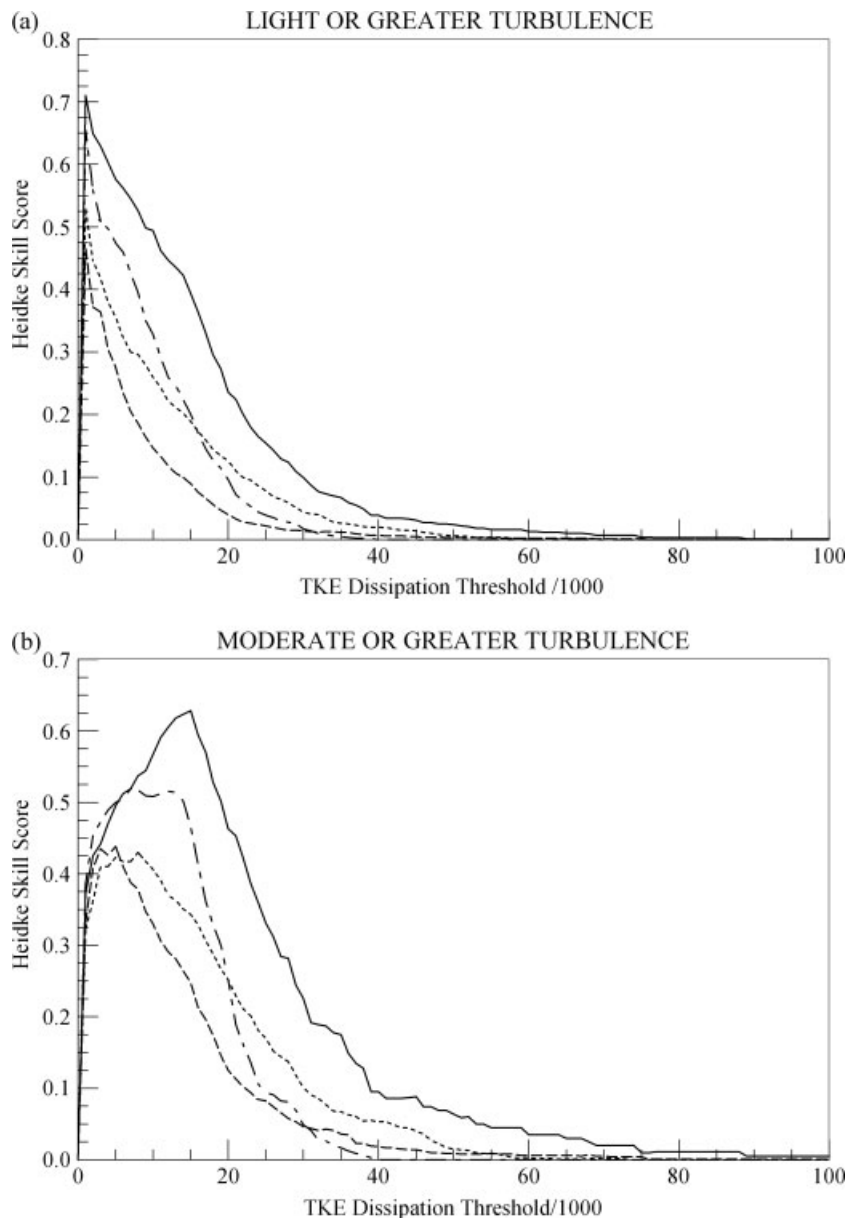
Figure 1. Heidke Skill Scores of (a) light or greater, and (b) moderate or greater PIREPs at various thresholds stratified by altitude using the TKE dissipation KMW method. PIREPs and forecasts were from November, 2005, through March, 2006. ——— Below FL100, – ‑ – ‑ FL100-FL190, ‑‑‑‑‑‑ FL200-FL290, ·········· FL300-FL500.

Table I. Standard mapping of eddy dissipation rate to subjective turbulence intensity from Pettegrew *et al.* (2010).

EDR($m^{2/3}$ s^{-1})	Intensity
0.15	Light
0.35	Moderate
0.55	Severe

4. ULTURB versus KMW

4.1. Methodology

A daily ULTURB forecast was computed from the 13 km horizontal resolution RUC2 numerical model from 25 September 2008 to 31 December 2008. The RUC2 forecasts were downloaded from the National Centers for Environmental Prediction ftp site with a 25 hPa vertical resolution. ULTURB output in each 25 hPa layer was assigned to one or more 1000 ft flight levels within the layer. For example, FL180 is within the 500–525 hPa layer and both FL350 and FL360 are within the 225–250 hPa layer. All forecasts were 3 h forecasts mostly from 1500 UTC that verified at 1800 UTC, but some forecasts verified at other times between 1600 UTC and 0100 UTC because of missing data. PIREPs were gathered within the RUC2 forecast domain, the conterminous United States of America, southern Canada, northern Mexico, and adjacent coastal waters, at or above FL100 for the period 1 h preceding and 1 h succeeding the verification time for the day. Most of the PIREPs reported turbulence at a single location and at a single flight level. However, if a PIREP reported turbulence

Table II. Intensity distribution of the 5315 pilot reports in the 2008 study database.

Intensity	Number
Smooth	1985
Light	1185
Light-moderate	457
Moderate	1610
Moderate-severe	45
Severe	33

between two points, it was counted as two reports, one at one-third the location difference between the two points and the other at two-thirds the difference. A multi-level PIREP was counted as a report in each of the 25 hPa thick layers it intersected.

PIREPs associated with any mountain waves indicated by the MWAVE algorithm (McCann, 2006) were removed. The MWAVE algorithm computes turbulence from mountain waves from a modified McFarlane (1987) parameterization of orographically induced wave drag into the free atmosphere. Because breaking wave drag causes turbulence above mountains, mountain wave influences in the CAT-only PIREP database needed to be minimized. For similar reasons, radar or satellite imagery was also analysed subjectively for convective patterns and any PIREPs in them removed. These procedures netted 5315 PIREPs; Table II shows the distribution of reported turbulence intensities. The highest ULTURB EDR value within 50 km of the PIREP were extracted.

Since there were few severe turbulence reports during the study period, this database was supplemented with 361 severe-only PIREPs gathered from 1 November 2009 to 31 March 2010 similarly to the original study but occurring at any time of day. ULTURB EDR values were assigned to each PIREP similarly as in the 2008 database.

4.2. Verification results

One way to assess an algorithm's skill is to create a set of 2×2 contingency tables by varying the threshold chosen to make a yes-or-no forecast decision and then comparing those with the yes-or-no observed conditions (Mason, 1982). For each threshold the members of the table are the number of correct 'yes' forecasts (YY), the number of correct 'no' forecasts (NN), the number of incorrect 'yes' forecasts (YN), and the number of unforecasted events (NY). With the probability of detection of 'yes' observations [$POD_{yes} = YY/(YY + NY)$] and the probability of false detection of 'no' observations [$POFD_{no} = YN/(NN + YN)$] receiver operating characteristic (ROC) curves (Mason and Graham, 1999) were created for light, moderate and severe turbulence for both ULTURB and the original KMW method. Because, as mentioned previously, there were only a small number of severe turbulence PIREPs in the 2008 database, the ULTURB severe ROC curve with the POD_{yes} statistics was produced by combining the severe-only 2009–2010
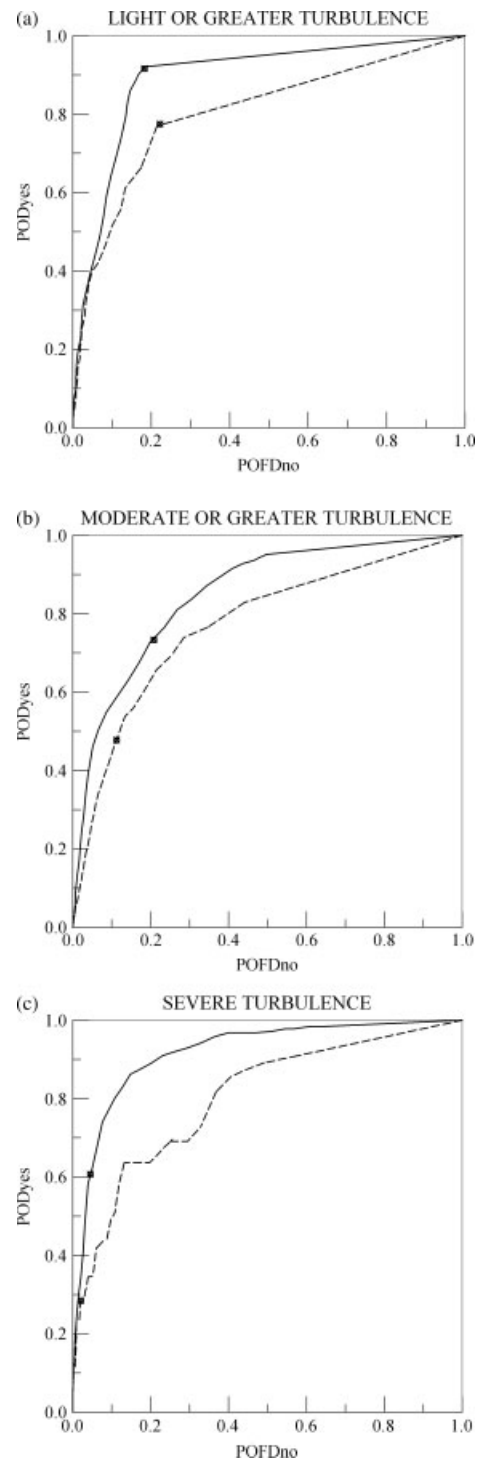

Figure 2. Receiver operating characteristic curves for (a) light or greater, (b) moderate or greater, and (c) severe turbulence for a set of daily ULTURB 3-h forecasts (solid) and similar KMW forecasts (dashed). The marker on each curve is the Table I threshold for each intensity. ----- KMW, ——— ULTURB.

database with the severe reports in the 2008 database and assuming that the 2008 $POFD_{no}$ statistics for severe turbulence are a representative sample of the ULTURB severe turbulence forecast population. The marker on each curve is the Table I threshold for that intensity. The closer that the ROC curve is to the upper left corner of the graph, the more skillful is the method.
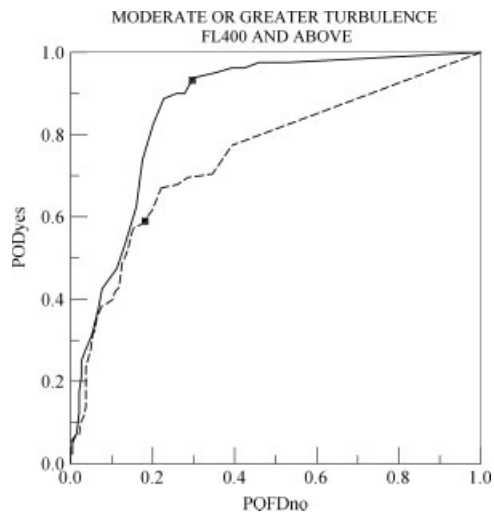
Figure 3. Receiver operating characteristic curves for moderate or greater turbulence for ULTURB forecasts (solid) and similar KMW forecasts (dashed) for pilot reports above FL400. The marker on each curve is the Table I threshold for each intensity. ----- KMW, ——— ULTURB.

As seen in Figure 2, ULTURB is clearly better than the original KMW method for all intensities indicating that the full accounting of the gravity wave-modified TKE equation outlined in Section 3.2 was beneficial. Figure 3 shows the ULTURB and KMW moderate or greater ROC curves for PIREPs at or above FL400 only. Again, ULTURB is an improvement over the KMW method which validates that the full accounting of the gravity wave-modified TKE equation improved the verification of PIREPs above the tropopause as intended.

5. ULTURB versus GTG2

The second version of the Graphical Turbulence Guidance product (GTG2) has higher skill than any other turbulence forecast method prior to KMW (Sharman *et al.*, 2006). Although KMW found its method superior to GTG's first version, it was not strictly a like-with-like comparison. With the 2008 5315 PIREP and 2009–2010 361 severe-only PIREP databases, it was possible to make a truer assessment. The Aviation Weather Center, Kansas City, Missouri, USA, provided corresponding GTG2 forecasts computed in the native isentropic vertical resolution from the same 13 km RUC2 forecasts in the 2008–2010 studies. The provided GTG2 grids were degraded to 20 km horizontal resolution and interpolated to 1000 ft vertical resolution between FL100 and FL450. GTG2 output is a non-dimensional number between zero and one. The verifying GTG2 forecast was extracted for each PIREP identically to the method outlined in Section 4. Therefore, each pilot report had a corresponding ULTURB and GTG2 forecast.

In Figure 4 ULTURB betters GTG2 at each turbulence intensity. As in the previous figures, the marker indicates the stated algorithm threshold for that intensity, i.e., Table I values for ULTURB and for GTG2 0.30 for
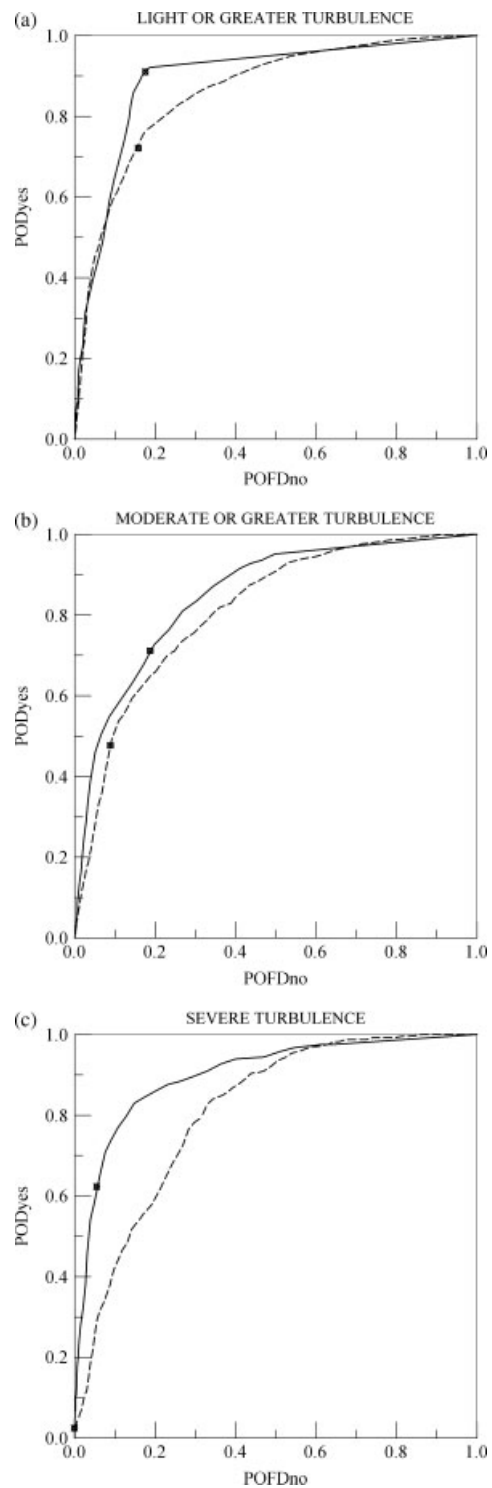

Figure 4. Receiver operating characteristic curves for (a) light or greater, (b) moderate or greater, and (c) severe turbulence for a set of daily ULTURB 3-h forecasts (solid) and similar GTG2 forecasts (dashed). The marker on each curve is each intensity's Table I threshold for ULTURB and the Sharman *et al.* (2006) threshold value for GTG2, respectively. ——— ULTURB, ----- GTG2.

light, 0.50 for moderate, and 0.80 for severe (Sharman *et al.*, 2006). GTG2 has substantial difficulties forecasting severe CAT. Less than 3% of all severe PIREPs had a GTG2 forecast greater than 0.80, and none of these PIREPs were above FL200.

6. Concluding remarks

The clear-air turbulence forecasting method introduced by Knox *et al.* (2008), hereafter KMW, has been modified. The primary modification, which we call ULTURB (Upper Level TURBulence), accounts for environmental wind shear and stability when appropriate. The KMW method was tested below FL200, and it skillfully forecasts turbulence intensity at those flight levels as well. Thus, ULTURB forecasts turbulence at all flight levels above the top of the planetary boundary layer. The KMW output metric from TKE dissipation was cosmetically transformed into eddy dissipation rate.

ULTURB's core remains identical to the KMW method. Its dynamical approach is a logical progression to improve CAT (clear air turbulence) forecasting and has the potential to establish a firmer foundation for it. If its success is indeed rooted in spontaneous emission of gravity waves initiating turbulence, this could provide forecasters with considerable physical insight. Since this approach is relatively simple and dynamically self-consistent, forecasters could intelligently add value to guidance forecasts such as ULTURB. Currently, a forecaster wanting to add value to a GTG forecast has to have diagnoses of each its inputs and then guess at their relative importance.

ULTURB is a superior forecast method to GTG2, especially for severe turbulence for which GTG2 apparently has difficulty forecasting at jet aircraft cruising altitudes. Additionally, ULTURB skillfully forecasts CAT below FL100 while GTG2 does not. Since the future of GTG is to be a one-stop-shop for all forms of turbulence, it is recommended that the GTG developers use ULTURB as GTG's CAT component.

There is still substantial room to improve ULTURB. Lighthill–Ford radiation is unlikely to be the only source for atmospheric gravity waves. For example, Plougonven and Zhang, (2007) describe an alternate forcing source based on the vertical gradients of the nonlinear balance equation, the sum of vorticity advection and the Coriolis parameter times divergence, and the Laplacian of temperature advection. Their equations have yet to be computed on actual atmospheric data as in KMW. It is not known whether their method would yield similar results as or is independent of KMW's application of Lighthill–Ford theory. Additionally, inertia-gravity waves may propagate substantial distances from their source complicating wave analyses, and there are wave-mean flow and wave-to-wave interactions (Benney, 1977; Franke and Robinson, 1999) and even wave-turbulence interactions (Fua *et al.*, 1982). Furthermore, mountainous areas of the western United States are prone to more CAT than other areas (Wolff and Sharman, 2008). While that area is prone to significant mountain wave activity, on a case-by-case basis it is often tricky to distinguish between the turbulence due to a mountain wave and a clear-air mechanism. Since both are caused by gravity waves, it is not difficult to envision that both wave sources may combine to create a stronger event than either could individually.

Aviation professionals and the flying public need better forecasts to help reduce the substantial costs and injuries due to inflight turbulence. It is hoped that this work leads to a better understanding and operational predictions of CAT.

Acknowledgements

References

Benney DJ. 1977. A general theory for interactions between short and long waves. *Studies in Applied Mathematics* **56**: 81–94.

Cornman LB, Meymaris G, Prestopnik J, Tasset T. 2008. An update on turbulence reporting from commercial aircraft. *Proceedings 13th Conference on Aviation, Range, and Aerospace Meteorology*. American Meteorological Society: Boston, MA; paper 10.1. http://ams.confex.com/ams/88Annual/techprogram/paper_135610.htm

Doswell CA III, Davies-Jones R, Keller D. 1990. On summary measures of skill in rare event forecasting based on contingence tables. *Weather and Forecasting* **5**: 576–585.

Dunkerton TJ. 1997. Shear instability of inertia-gravity waves. *Journal of Atmospheric Sciences* **54**: 1628–1641.

Dutton MJO. 1980. Probability forecasts of clear-air turbulence based on numerical model output. *Meteorological Magazine* **109**: 293–309.

Dutton JA, Panofsky HA. 1970. Clear air turbulence: a mystery may be unfolding. *Science* **167**: 937–944.

Ellrod GP, Knapp DI. 1992. An objective clear-air turbulence forecasting technique: verification and operational use. *Weather and Forecasting* **7**: 150–165.

Ford R. 1994. Gravity wave radiation from vortex trains in rotating shallow water. *Journal of Fluid Mechanics* **281**: 81–118.

Franke PM, Robinson WA. 1999. Nonlinear behavior in the propagation of atmospheric gravity waves. *Journal of Atmospheric Sciences* **56**: 3010–3027.

Fua D, Chimonas G, Einaudi F, Zeman O. 1982. An analysis of wave-turbulence interactions. *Journal of Atmospheric Sciences* **39**: 2450–2463.

Garratt JR. 1992. *The Atmospheric Boundary Layer*, Cambridge University Press: Cambridge, UK; 316.

Knox JA. 1997. Possible mechanisms of clear-air turbulence in strongly anticyclonic flows. *Monthly Weather Review* **125**: 1251–1259.

Knox JA, McCann DW, Williams PD. 2008. Application of the Lighthill-Ford theory of spontaneous imbalance to clear-air turbulence forecasting. *Journal of Atmospheric Sciences* **65**: 3292–3304.

Knox JA, McCann DW, Williams PD. 2009. Reply to Plougonven, *et al.*'s "Comments on 'Application of the Lighthill-Ford theory of spontaneous imbalance to clear-air turbulence forecasting'". *Journal of Atmospheric Sciences* **66**: 2511–2516.

Lighthill MJ. 1952. On sound generated aerodynamically, I General theory. *Proceedings of the Royal Society of London* **211A**: 564–587.

McCann DW. 1999. A simple turbulent kinetic energy equation and aircraft boundary layer turbulence. *National Weather Digest* **23**(1–2): 13–19.

McCann DW. 2001. Gravity waves, unbalanced flow, and clear air turbulence. *National Weather Digest* **25**(1–2): 3–14.

McCann DW. 2006. Diagnosing and forecasting aircraft turbulence with steepening mountain waves. *National Weather Digest* **30**: 77–92.

McFarlane NA. 1987. The effect of orographically excited gravity wave drag on the general circulation of the lower stratosphere and troposphere. *Journal of Atmospheric Sciences* **44**: 1775–1800.

Mason I. 1982. A model for assessment of weather forecasts. *Australian Meteorological Magazine* **30**: 291–303.

Mason SJ, Graham NE. 1999. Conditional probabilities, relative operating characteristics and relative operating levels. *Weather and Forecasting* **14**: 713–725.

Miles JW, Howard LN. 1964. Note on a heterogeneous flow. *Journal of Fluid Mechanics* **20**: 331–336.

Pettegrew B, Loughe AF, Hart JE, Mahoney JL, Henderson JK, Hart JE. 2010. On the use of eddy dissipation rate observations in verification. *Proceedings 14th Conference on Aviation, Range, and Aerospace Meteorology*. American Meteorological Society: Boston, MA; paper P473, http://ams.confex.com/ams/90annual/techprogram/paper_161489.htm

Plougonven R, Snyder C, Zhang F. 2009. Comments on "Application of the Lighthill-Ford theory of spontaneous imbalance to clear-air turbulence forecasting". *Journal of Atmospheric Sciences* **66**: 2506–2510.

Plougonven R, Zhang F. 2007. On the forcing of inertia-gravity waves by synoptic-scale flows. *Journal of Atmospheric Sciences* **64**: 1737–1742.

Sharman R, Tebaldi C, Wiener G, Wolff J. 2006. An integrated approach to mid- and upper-level turbulence forecasting. *Weather and Forecasting* **21**: 268–287.

Williams PD, Haine TWN, Read PL. 2005. On the generation mechanisms of short-scale unbalanced modes in rotating two-layer flows with vertical shear. *Journal of Fluid Mechanics* **528**: 1–22.

Williams PD, Haine TWN, Read PL. 2008. Inertia-gravity waves emitted from balanced flow: observations, properties, and consequences. *Journal of Atmospheric Sciences* **65**: 3543–3556.

Wolff JK, Sharman RD. 2008. Climatology of upper-level turbulence over the contiguous United States. *Journal of Applied Meteorology and Climatology* **47**: 2198–2214.